Astronomy & Astrophysics manuscript no. CPD-3
June 4, 2009

The dynamical role of the circumplanetary disc in planetary migration.

Aurélien Crida[1,2], Clément Baruteau[3,4], Wilhelm Kley[1], and Frédéric Masset[3,5]

[1] Institut für Astronomie & Astrophysik, Abt. Computational Physics, Universität Tübingen, Auf der Morgenstelle 10, D-72076 Tübingen, Germany
[2] now at : DAMTP, University of Cambridge, Wilberforce Road, Cambridge CB3 0WA, UK
[3] Laboratoire AIM-UMR 7158, CEA/CNRS/Université Paris Diderot, IRFU/Service d'Astrophysique, CEA/Saclay, 91191 Gif-sur-Yvette Cedex, France
[4] now at : Astronomy and Astrophysics Department, University of California, Santa Cruz, CA 95064, USA
[5] ICF-UNAM, Av. Universidad s/n, Cuernavaca, Morelos, C.P. 62210, Mexico

June 4, 2009

ABSTRACT

Context. Numerical simulations of planets embedded in protoplanetary gaseous discs are a precious tool for studying the planetary migration ; however, some approximations have to be made. Most often, the selfgravity of the gas is neglected. In that case, it is not clear in the literature how the material inside the Roche lobe of the planet should be taken into account.
Aims. Here, we want to address this issue by studying the influence of various methods so far used by different authors on the migration rate.
Methods. We performed high-resolution numerical simulations of giant planets embedded in discs. We compared the migration rates with and without gas selfgravity, testing various ways of taking the circum-planetary disc (CPD) into account.
Results. Different methods lead to significantly different migration rates. Adding the mass of the CPD to the perturbing mass of the planet accelerates the migration. Excluding a part of the Hill sphere is a very touchy parameter that may lead to an artificial suppression of the type III, runaway migration. In fact, the CPD is smaller than the Hill sphere. We recommend excluding no more than a 0.6 Hill radius and using a smooth filter. Alternatively, the CPD can be given the acceleration felt by the planet from the rest of the protoplanetary disc.
Conclusions. The gas inside the Roche lobe of the planet should be very carefully taken into account in numerical simulations without any selfgravity of the gas. The entire Hill sphere should not be excluded. The method used should be explicitly given. However, no method is equivalent to computing the full selfgravity of the gas.

Key words. Methods: numerical — (Stars): planetary systems: formation — Accretion, accretion discs

1. Introduction

Planetary migration has been widely studied in the past decade, after the discovery of the first exoplanets. Indeed, the first known exoplanets were mostly hot Jupiters that could not have formed where they presently orbit, according to the standard theory of planet formation. Consequently, they are supposed to have migrated in the protoplanetary gaseous disc before its dissipation. More recently, pairs of exoplanets in mean motion resonance have been detected. This particular configuration requires some dissipative process for the planets to approach each other and lock in resonance. This is a strong evidence for planetary migration.

The theory of planetary migration was in fact proposed before the observational evidence (Goldreich & Tremaine 1979; Lin & Papaloizou 1979; Meyer-Vernet & Sicardy 1987; Lin & Papaloizou 1986b; Ward 1986). Numerical simulations allow study of more complex cases (several planets for instance) and refinement of our understanding of this phenomenon. Therefore, numerical studies of planetary migration are numerous in the literature. De Val-Borro et al. (2006) have compared the results of various codes on two typical test problems and find an overall consistency between the codes ; however, a few numerical and physical issues are still open. In particular, a circumplanetary disc (CPD) generally appears around giant planets. Without mesh refinement, this structure is generally poorly resolved, but still present. As it lies close to the planet, it could potentially exert a strong force on it. So far, a very limited number of studies have considered the probably important role of the CPD in the migration rate. As this material is considered to belong to the planet and in order to avoid numerical artifacts due to the small distance, some authors exclude the Hill sphere of the planet from the calculation of the force of the gas on the planet. Most authors identify the CPD with the Hill sphere, which in fact does not hold as we shall see below (see also D'Angelo et al. 2005). Some authors add the mass of the gas in the Hill sphere to the planet mass when computing the planet gravity field. Others add the acceleration caused by the entire gas disc on the planet to the gas in the Hill sphere. In fact, the situation is confused, and there is no consensus on this issue.

Recently, Crida et al. (2008) have shown how planetary migration can explain the orbital parameters of exoplanets in mean motion resonance, and remarked that the outcome of their simulations had a dependence on the way they deal with the gas in the Hill sphere of the planets. Pepliński et al. (2008) have also

Send offprint requests to: A. Crida,
crida@tat.physik.uni-tuebingen.de

enlightened that the role of the CPD is not a minor one, and that a careful study of this problem is needed to answer this question.

In this paper, we study the influence of the CPD on the planetary migration in numerical simulations. The theory is discussed, to get a better understanding of the problem. This leads to possible solutions to treat the CPD. We perform 2D simulations with modest to high resolution, and we test and compare various recipes. Our goal is to provide a survey of the parameter "CPD" in numerical simulations. In particular, the fraction of the Hill sphere that is excluded is a very touchy parameter, and the way the exclusion is performed has a great influence on the outcome of the simulation. Many authors are not aware of this. Our survey shows that some popular methods are inappropriate. We present better ways of dealing with the material present in the Hill sphere, in particular the CPD.

This requires an analysis of the Hill sphere structure, but in the framework of global disc simulations, which are not dedicated to resolve the Hill sphere with a high level of precision. We do not aim at understanding the detailed physics and the fine structure of the CPD itself, but more how the gas in the Hill sphere of the planet should be taken into account. Convergence properties and the impact of varied prescriptions on the equation of state (EOS) or the softening length are fundamental issues, but we do not address them in this work. Instead, our aim is to find an adequate prescription for the torque calculation in non self-gravitating simulations, based on general considerations such as the conservation of angular momentum and the main features of the flow topology in the vicinity of the planet. The conservation of angular momentum is enforced in our scheme independently of the resolution, while the flow topology depends very weakly on the resolution (even if the mass of the CPD does, in an EOS-dependent way).

This paper is organised as follows. In Sect. 2, the problem is explained and analysed. Some definitions are provided, in order to clarify the strategy and the questions that arise from the presence of a CPD. We show that the problem can be divided into the questions of the *perturbing mass*, of the *gravitational mass*, and of the *inertial mass* of the planet. In Sect. 3, the numerical setup is presented. Then, in the following sections, numerical experiments are performed. In Sect. 4, a Jupiter mass planet, in type II migration in considered. In Sect. 5, the influence of the CPD on a Saturn mass planet, in type III migration is studied. In Sect. 6, the structure of the Hill sphere is analysed in detail, and the size of the CPD is estimated. Last, our results are summarised, and we conclude in Sect. 7.

2. Problem presentation

2.1. Disc structure

Let us consider a planet on a circular orbit around a central star. In steady state, in the frame corotating and drifting along with the planet, the gaseous disc is split into 4 closed regions :

1. The *Roche lobe* of the planet, which is where the streamlines are closed around the planet. In the restricted three-body problem, it can be approximated by the *Hill sphere*, centred on the planet, of radius the Hill radius : $r_H = a_p(q/3)^{1/3}$, which is where a_p is the semi-major axis of the planet and $q = M_p/M_*$ is the ratio of the planet and stellar masses.
2. The *horseshoe region* around the orbit of the planet, where the streamlines have a horseshoe shape. This region is delimited by the horseshoe *separatrices*.
3. The *inner disc* between the star and the horseshoe inner separatrix.
4. The *outer disc* beyond the horseshoe outer separatrix.

The Roche Lobe disappears for low-mass planets ($q \lesssim 10^{-4}$, but this depends on the aspect ratio, see Masset et al. 2006, Fig. 11).

The gas in the inner disc and in the outer disc exert a torque on the planet, the *differential Lindblad torque*. The gas present in the horseshoe region exerts the so-called *horseshoe drag* (Ward 1991; Masset 2001). For low-mass planets in locally isothermal discs, the sum of these two effects is generally a negative torque and responsible for type I planetary migration (Ward 1997). If the energy equation is taken into account, the torque due to the horseshoe drag is modified in radiatively inefficient discs as well as in more realistic radiative discs. This may slow down or reverse the type I migration (Paardekooper & Mellema 2006; Baruteau & Masset 2008a; Kley & Crida 2008). For intermediate mass planets, under some circumstances, the horseshoe drag can also be responsible for type III migration (Masset & Papaloizou 2003).

The effect of the gas present in the Roche lobe of the planet has so far been neglected by most authors (with the noticeable exceptions of D'Angelo et al. 2005; Pepliński et al. 2008, see below), and never explicitly analysed. However, as this material is located very close to the planet, it could exert on it a strong force and torque. Consequently, it has to be carefully taken into account. We show further that it can influence the migration rate by almost a factor 2. This concerns planets of sufficient mass, which are able to create a Roche lobe in the disc and to accrete gas.

Please note that the CPD does not necessarily fill the entire Hill sphere. There may be material inside the Hill sphere that is not orbiting around the planet, but that is simply passing by. D'Angelo et al. (2005); Pepliński et al. (2008) have shown that the gas dynamics around a migrating planet is more complicated than described in Sect. 2.1, and that the Roche lobe may be modified. This may be a source of confusion. Hereafter, the CPD always refers to the material bound to the planet – that is : on a streamline that describes an orbit around the planet – while the Hill sphere refers to the material located within a distance r_H to the planet.

2.2. Gravitational interactions

In Fig. 1 are displayed all the gravitational interactions physically present in the problem. The gaseous disc has been split into the CPD, which is the gas orbiting the planet, bound to the planet, and the rest of the ProtoPlanetary Disc (PPD). Four systems are interacting with each other, which makes a total of 12 interactions. In addition, the PPD and the CPD, as extended systems, exert on themselves a gravity force.

These 14 gravitational actions can be classified in 4 categories :

- **5 direct terms** (red solid arrows) : The Planet→PPD, Planet→CPD, Star→PPD, Star→CPD, Star→Planet are the most essential interactions of the system. They are responsible for the disc and planet orbiting the star and for the perturbations of the disc, including the mere existence of the CPD.
- **3 indirect terms** (red dashed arrows) : The (re)actions of the PPD, the CPD, and the planet on the star are generally considered as indirect terms in the expression of the potential, if the frame is centred on the star.
- **4 selfgravity terms** (blue dotted arrows) : All the interactions between parts of the gaseous disc belong to what is

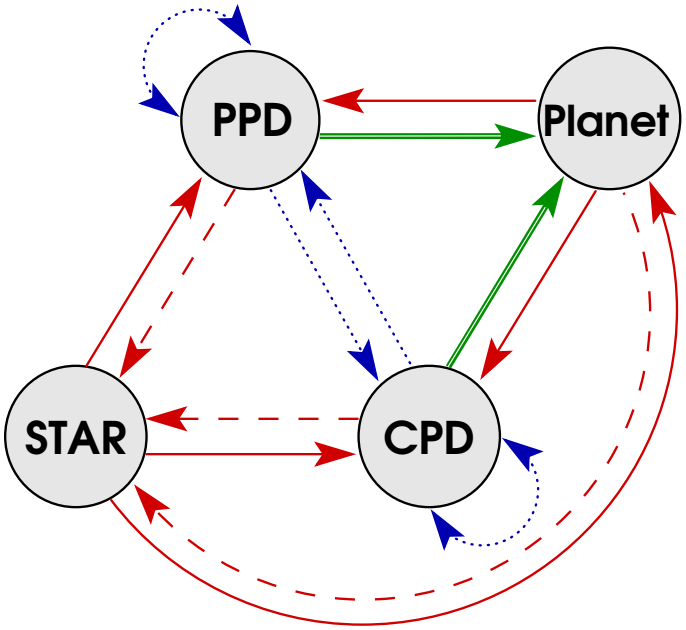

Fig. 1. Summary of the gravitational interactions in the problem of a planet, surrounded by a CPD, orbiting in a PPD, about a star.

called the selfgravity of the disc (PPD→PPD, PPD→CPD, CPD→PPD, CPD→CPD).

– **2 migration terms** (green double arrows) : The action of the disc (PPD and CPD) on the planet are responsible for the planetary migration.

If all the 14 interactions were taken into account in the simulations, the computations would be self-consistent. The interactions of the two first categories are always taken into account and are clearly understood. But the selfgravity is generally not computed, because it is too expensive in terms of CPU-time. Consequently, the 2 migration terms may be inaccurate.

The PPD⟷PPD effects, which is the influence of the gas selfgravity on the differential Lindblad torque, has been studied for low-mass planets by Nelson & Benz (2003), Pierens & Huré (2005), and more recently by Baruteau & Masset (2008b,c). They confirmed that the type I migration is slightly accelerated by the disc selfgravity. This effect is not discussed here. On the contrary, we only focus on the effect of the CPD.

In this paper, we plan to analyse the role and the behaviour of the CPD in the migration, which is represented by the arrows CPD→Planet, CPD→PPD, and PPD→CPD. As already said, the action Planet→CPD should always be present and is not in question. In simulations with full gas selfgravity computed, all the blue dotted arrows of Fig. 1 are taken into account, including the CPD↔CPD arrow. However, the selfgravity of the CPD should only give a minor change of the CPD structure. It should therefore be negligible for what concerns the planetary migration. In what follows, we do not discuss the role of the CPD↔CPD gravitational interaction.

2.3. Effect of the circumplanetary disc on the planet

The presence of a CPD, gravitationally bound to the planet, can affect the migration by three means :

1. CPD→Planet : External perturbations (Star→CPD, PPD→CPD) make the CPD not axisymmetric around the planet. Thus, the CPD could exert a torque on the planet ; we call this torque due to the CPD structure a *direct torque*.
2. CPD→PPD→Planet : By perturbing the PPD, the CPD influences the action of the latter on the planet. Basically, the CPD acts like the planet does, enhancing the amplitude of the perturbation. We define this as the *perturbing mass problem*.
3. CPD→Planet in migration : The planet and all the material that is bound to it migrate together. During the migration, the CPD is still linked to the planet. Consequently, the CPD is like a ball and chain for the planet. If the full gas selfgravity is computed, the CPD feels almost the same specific torque from the PPD than the planet ; then, the ball is pulled by the PPD, together with the planet, and the chain is not taut. If the full gas selfgravity is not computed (no blue arrow in Fig. 1), the CPD feels no torque from the PPD and tends to stay on a constant orbit. Then, the migrating planet has to pull the CPD. The chain is taut, which slows down the planetary migration. We define this as the *inertial mass problem*.

The first and third cases are included in the green, double arrow CPD→Planet in Fig. 1. The force acting on the planet in these two cases arises from gravitational interaction with the gas located in the CPD itself.

The second case is an indirect interaction, represented in Fig. 1 by the two-arrow path : CPD→PPD→Planet. The action of the CPD on the PPD (blue dotted arrow CPD→PPD) may change the value of the green double arrow PPD→Planet.

2.4. Problem analysis and possible solutions

In this paper, we evaluate either the specific torque felt by the planet T_p or the migration rate $\dot{a}_p$ (the dot denotes the derivative with respect to time). Both quantities are equivalent, as for a planet on a circular orbit, $2a_p\dot{a}_pB = T_p$, with B the second Oort constant.

It is well-known that a planet orbiting in a gaseous PPD perturbs the latter gravitationally. In the linear regime, this perturbation leads to the appearance of a one-armed spiral wave, called the *wake*, in the inner and the outer discs. The amplitude of the perturbation is proportional to the planet mass M_p. The perturbed density distribution leads to a gravitational force on the planet. This force is proportional to the mass of the wake times the mass of the planet *i.e.* proportional to ${M_p}^2$. Thus, the planet feels from the disc a torque proportional to its mass squared. As a result, the specific torque applied to the planet is proportional to the planet mass M_p. This corresponds to the PPD⇆Planet arrows in Fig. 1.

If the planet is surrounded by a CPD, things are slightly different. Indeed, the CPD is gravitationally bound to the planet, and it moves with the planet. Thus, the planet of the above paragraph should be replaced by the planet and its CPD. The specific torque felt by this system is proportional to $(M_p + M_{\rm CPD})$, where $M_{\rm CPD}$ is the mass of the CPD. The presence of the CPD should increase the migration speed.

More generally, the specific torque felt by the migrating body is proportional to the amplitude of the perturbation of the disc (proportional to the *perturbing mass* of the planet), times the mass of the body gravitationally interacting with it (*gravitational mass* of the planet), divided by the mass of the migrating body (*inertial mass* of the planet). If selfgravity is computed, these three masses are equal to $(M_p + M_{\rm CPD})$. However, as we see below, the perturbing, gravitational, and inertial masses of the

planet differ if the gas selfgravity is not computed. This is the problem.

In numerical simulations without gas selfgravity, the CPD does not perturb the PPD, neither does it feel a torque from it : in Fig. 1, the blue dotted arrows are suppressed. The perturbing mass is M_p, and the force felt by the planet is proportional to ${M_p}^2$. But the CPD is linked to the planet. To follow the planet in its migration, the CPD has to exchange angular momentum with it. Thus, the relevant inertial mass of the planet is not M_p but $(M_p + M_{\rm CPD})$. The specific torque felt by the migrating system (the planet and its CPD) is proportional to ${M_p}^2/(M_p + M_{\rm CPD})$. Here, the presence of the CPD decreases the migration speed, which should not occur.

Based on this analysis, several authors (e.g. Pierens & Nelson 2008) have tried to cancel the force from the CPD on the planet by excluding the Hill sphere of the computation of the force of the disc on the planet. This aims at suppressing the green double arrow CPD→Planet in Fig. 1. Thus, the inertial mass of the planet is M_p again, and one is back to the first case ; the specific torque is proportional to M_p, but not to $(M_p + M_{\rm CPD})$.

Others (e.g. Masset 2006; Pepliński et al. 2008) have suggested adding $M_{\rm CPD}$ to the perturbing mass of the planet (denoted M_p^* by Pepliński et al.), to make the amplitude of the wake proportional to $(M_p + M_{\rm CPD})$. In Fig. 1, this is equivalent to adding the blue, dotted CPD→PPD arrow. This gives a torque proportional to $(M_p + M_{\rm CPD})M_p$ and a specific torque proportional to $(M_p + M_{\rm CPD})M_p/(M_p + M_{\rm CPD}) = M_p$ as well. Pepliński et al. (2008) find very little change in the migration rate by using M_p or $(M_p + M_{\rm CPD})$ as the perturbing mass of the planet, which is quite surprising, as they have $M_{\rm CPD} \sim M_p$.

By adding $M_{\rm CPD}$ to the planet mass felt by the disc (the perturbing mass) and excluding the CPD from the disc felt by the planet, one should recover a specific torque proportional to $(M_p + M_{\rm CPD})M_p/M_p = (M_p + M_{\rm CPD})$. One could also think of adding $M_{\rm CPD}$ to the perturbing mass of the planet and to the gravitational mass of the planet. In that case, the torque is proportional to $(M_p + M_{\rm CPD})^2$. As the inertial mass is $(M_p + M_{\rm CPD})$, we find a specific torque in $(M_p + M_{\rm CPD})$, as required.

Pepliński et al. (2008) have already addressed this issue and quite clearly described the problem. In the frame of type III migration, they argue against any exclusion of a part of the disc in the torque calculation, but they propose another solution by applying the acceleration felt by the planet from the disc to the CPD (see their Eqs. (13) and (17)). This should mimic the blue, dotted arrow PPD→CPD. In their paper, this acceleration is given by all the disc, CPD included. Then, if the CPD exerts, say, a positive torque on the planet for whatever reason, this positive contribution will be applied to the CPD as well. This should not be, because it opens the possibility for the CPD to pull the planet indefinitely, without losing any angular momentum. For consistency, the acceleration applied to the CPD should be the one felt by the planet from the PPD, CPD excluded : the green, double arrow PPD→Planet in our Fig. 1.

The giant planets studied in this paper are not in the linear regime, so that the torque is not exactly proportional to ${M_p}^2$. However, this approximation allows the above reasoning. It enlightens the role of the CPD in the migration process and suggests solutions. In Sects. 4 and 5, we numerically test these recipes and compare them with the results obtained with full selfgravity.

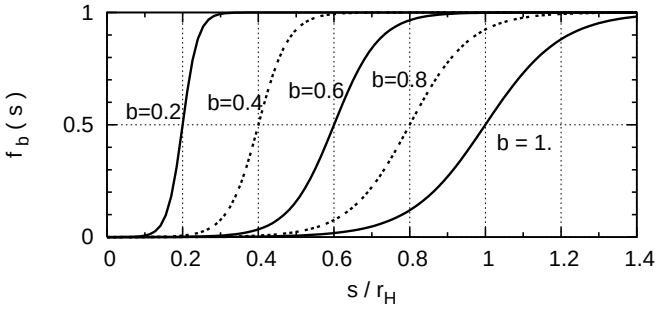

Fig. 2. The function $f_b(s)$ given by Eq. (3) for various values of b.

3. Code and setting description

To compare the migration rates obtained with different prescriptions to take the CPD into account, we performed numerical simulations, using the code FARGO (Masset 2000a,b). This is a publicly available[1] 2D code, using polar coordinates (r, θ). We used the ADSG version, in which the energy equation and the gas selfgravity are implemented. The gas selfgravity is described in Baruteau & Masset (2008c). It can be turned on or off.

The uniform kinematic viscosity is $\nu = 10^{-5}\, {a_p}^2 \Omega_p$ (Ω_p being the angular velocity of the planet and a_p its semi major axis). The initial aspect ratio is $h_0 = (H/r)_0 = 0.03$. To take the disc thickness into account, a smoothing length $\epsilon = 0.018\, a_p$ (60% of the initial disc height) is used in the expression of the planet potential Φ_p :

$$\Phi_p = -\frac{GM_p^*}{s'}\,, \tag{1}$$

where $s' = \sqrt{s^2 + \epsilon^2}$ with s the distance to the planet, and M_p^* is the perturbing mass of the planet, equal to M_p if not otherwise specified.

The vector force $\boldsymbol{F}_{\boldsymbol{p},b}$ exerted by the disc on the planet is computed using the following expression :

$$\boldsymbol{F}_{\boldsymbol{p},b} = \int_{s=0}^{+\infty}\int_{\theta=0}^{2\pi} \frac{GM_p\Sigma}{s'^3} f_b(s)\boldsymbol{s}\,{\rm d}\theta\,{\rm d}s\,, \tag{2}$$

where $\boldsymbol{s}$ is the vector originating from the planet to the centre of the considered cell. The force $\boldsymbol{F}_{\boldsymbol{p},b}$ depends of the parameter b through the term $f_b(s)$: this is our filter used to exclude smoothly the neighbourhood of the planet, if necessary, also used in Crida et al. (2008). It is a smooth increasing function from 0 at $s = 0$ to 1 when $s \to \infty$ through 1/2 when $s = b\, r_H$, drawn in Fig. 2, and given by:

$$f_b(s) = \left[\exp\left(-10\left(\frac{s}{br_H} - 1\right)\right) + 1\right]^{-1}\,. \tag{3}$$

For $s < br_H$, $f_b(s) \ll 1$, while $f_b(s) \sim 1$ for $s > br_H$, so that the gas within a distance br_H of the planet is neglected while the gas outside is taken into account. For $b = 0$, $f_0 \equiv 1$, so that all the disc is taken into account ; $b = 0$ gives the standard expression of the force, with no exclusion of any part of the disc.

The planet is not accreting.

In the energy equation, the heat source is the viscous dissipation, and the cooling follows the following law, different from the public version of FARGO-ADSG :

$$\frac{\partial e}{\partial t} = -\sigma_R T^4/\kappa\Sigma\,, \tag{4}$$

[1] http://fargo.in2p3.fr/

Table 1. Resolution of the simulations.

time [orbits]	resolution $N_{\rm rings} \times N_{\rm sectors}$	$\delta r/r = \delta\theta$	designation
from 0 to 150 :	115 x 393	0.016	initialisation
from 150 to 250 :	230 x 786	8×10^{-3}	low
from 250 to 325 :	460 x 1572	4×10^{-3}	middle
from 325 to 400 :	920 x 3144	2×10^{-3}	high
from 400 to 477 :	1840 x 6288	10^{-3}	very high

where e is the thermal energy of the gas per unit area, σ_R is the Stefan-Boltzmann constant, T is the temperature, Σ is the surface density of the gas, and κ is the opacity, given by :

$$\kappa = \sigma_R \frac{8h_0^8}{9{\Sigma_0}^2\nu} . \quad (5)$$

This arbitrary constant opacity κ ensures that, in the absence of perturbation, the initial state is in thermodynamic equilibrium with a density profile $\Sigma(r) = \Sigma_0 r^{-1/2}$. Our equation of state is then, with c_s the sound speed, μ the mean molecular weight, R the universal gas constant, and $\gamma = 1.4$ the adiabatic index :

$$P = \Sigma {c_s}^2/\gamma = \Sigma \frac{RT}{\mu} . \quad (6)$$

The computation of the energy equation provides more realistic discs. In addition, it reduces the problem of the accretion of the CPD. Indeed, with a locally isothermal EOS, no pressure effect stops the collapse of the CPD. Then, at high resolution, gas in the neighbourhood of the planet reaches extremely high densities, and convergence is hard to obtain. Since we plan to increase gradually the resolution of our simulations (see next paragraph), we need a viscous and a compressional heating and a radiative cooling for the CPD structure to remain within reasonable limits of density and temperature. In addition, preliminary tests show that with the gas's full selfgravity and locally isothermal EOS, we could not reach convergence of the mass inside the Hill sphere. This motivated us to treat the gas thermodynamics. Our opacity is admittedly not realistic, and another prescriptions for κ would make the CPD larger or smaller. Once again, we are not interested in the true structure of the CPD in this study, but we simply want a stationary CPD, of reasonable size, to check how it influences the migration.

The radial grid extent is $r \in [0.4a_p; 2.5a_p]$. The regions $[0.4a_p; 0.5a_p]$ and $[2.1a_p; 2.5a_p]$ are wave-damping regions, in which the density, the temperature, and the velocities are damped toward the initial values. The rings are geometrically spaced and the cells squared : $\delta r/r = \delta\theta$ is constant. To save computing time, the resolution is initially low, and regularly doubled (see Table 1). In the end, a resolution of $N_{\rm rings} \times N_{\rm sectors} = 1840 \times 6288$ and $\delta r/r = \delta\theta = 10^{-3}$ is reached. To our knowledge, this is the first time that the FARGO code is run at such a resolution. Most of the very-high-resolution simulations were run on a parallel cluster with 64 CPUs. The FARGO code uses a staggered mesh, with the density and temperature evaluated at the centre of the cells, and the velocities at the boundaries. When the resolution is doubled, each cell is divided into four. The new values of the fields were computed with a 2D linear interpolation on the old grid.

Some remarks concerning the gas selfgravity are in order. The ADSG version of the FARGO hydro-code enables switching on or off the gas selfgravity, the computation of which is described in Baruteau & Masset (2008c). In addition, it is possible to compute only the axisymmetric component of the gas gravity. This is the gravity field caused by the azimuthally averaged density field of the gas, or by an axisymmetric disc with the same density profile as the actual gas disc. This component of the gas gravity field is responsible for increasing the angular velocity of the planet and of the gas itself (at least far enough from the disc inner edge). If one abruptly switches on the gas selfgravity when restarting a simulation computed without selfgravity, a discontinuity in the velocities is introduced. To avoid this, all our simulations are computed with the axisymmetric component of the gas gravity taken into account. This has a negligible computational cost, while the full selfgravity is quite expensive. As discussed in Baruteau & Masset (2008c), accounting for the axisymmetric component of the disc gravity has only a marginal effect on the Lindblad torque with respect to the situation where the planet is held on a fixed circular orbit in a non selfgravitating disc. In the cases that we study here, the planet is massive enough to shape a (deep or shallow) gap in the disc and to have a CPD. Consequently, the effect of selfgravity is different from in the above-mentioned studies. The shift of Lindblad resonances – which is essentially the only effect in type I migration – is taken over by the question of the gap shape, which gives the gas density at the position of each resonance, hence the torque. In addition, there are other issues, such as a modification of the perturbing, gravitational, and inertial mass of the planet, which we will address here.

4. Type II migration case

Following the procedure described in Sect. 3, we performed simulations of a Jupiter mass planet, with gas initial surface density : $\Sigma_0(r) = 10^{-4}(r/a_p)^{-1/2}\ M_*/{a_p}^2$. In this case, the planet opens a deep gap (Lin & Papaloizou 1986a; Crida et al. 2006), and the disc mass is low enough for type III migration not to happen (Fig. 12 of Masset & Papaloizou 2003). Thus, the planet should migrate in type II migration (Lin & Papaloizou 1986b). This choice could look inappropriate, because in standard type II migration, the migration speed is independent of the planet mass. However, this stands only if the disc is massive enough to push the planet at the viscous accretion speed. This occurs when $\mu > q/4$, where $\mu = 4\pi {a_p}^2\Sigma_0/M_*$ and $q = M_p/M_*$ (Crida & Morbidelli 2007; Crida 2006). Here, $q > 4\mu$, the disc is not massive enough for the migration to occur at a viscous rate. Consequently the migration rate should decrease with the inertial mass of the planet. This case is timely for studying our problem.

4.1. Inertial mass problem

As explained in Sect. 2.3, this problem only concerns migrating planets. To study this effect, we let the planet evolve freely in the disc. To test and quantify the influence of the CPD on the migration speed, a region around the planet is excluded from the computation of the force of the disc on the planet. To perform this, the parameter b in Eq. (2) is taken strictly positive, and several values are tested.

4.1.1. Middle resolution

First, the planet is released after 300 orbits on a fixed circular orbit ; the resolution of the grid is $\delta r = 4 \times 10^{-3}\, r = r_H/17.3$ (see Table 1), which is finer than the typical kind of resolution used in the literature. The migration is followed for 25 orbits. Various values of b from 0 to 1 are used. The results are displayed in

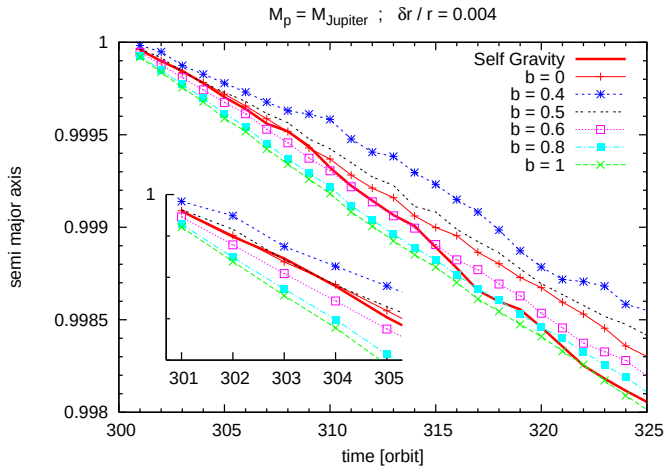

Fig. 3. Migration path of the Jupiter mass planet after its release at $t = 300$ orbits, with $\delta r/r = \delta\theta = 0.004$. The bold curve corresponds to a simulation where the full gas selfgravity is computed. The other ones come from simulations with exclusion of a part of the Hill Sphere, for various values of b. The first five orbits are enhanced in the inset at the bottom left.

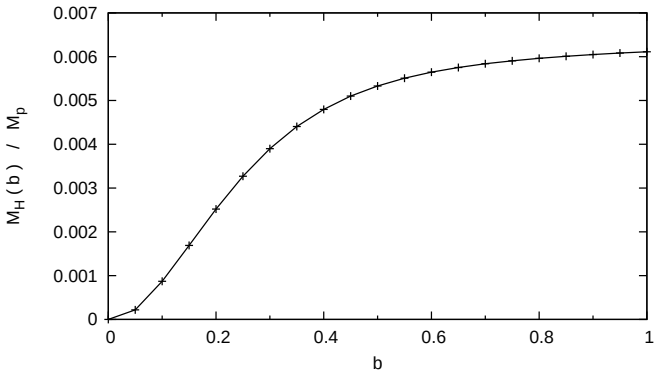

Fig. 4. Mass distribution inside the Hill sphere of the Jupiter mass planet given by Eq. (7), in planet mass units. The measure is made after 300 orbits on a fixed circular orbit, with a resolution of $\delta r/r = 0.004$.

Fig. 3. The curves for $b \leqslant 0.3$ almost overlap; therefore, only the curve for $b = 0$ is drawn as a thin red solid line with + symbols. For $b = 0.4$, the planet follows the blue starred line. It migrates significantly more slowly, and in 25 orbits, its semi-major axis has decreased 8.5% less. For $b \geqslant 0.4$, the migration speed increases with b, and for $b = 1$ (exclusion of all the Hill sphere), the semi-major axis of the planet decreases in 25 orbits nearly 12% more than in the case $b = 0$. The migration ratio after 10 orbits between $b = 0.4$ and $b = 1$ is almost 2. This shows that the Hill sphere can have a strong influence on the migration rate in numerical simulations.

The bold solid red curve in Fig. 3 is obtained with a simulation where the full selfgravity of the gas has been taken into account, while only the axisymmetric component is used in the others. Of course, in that case, no exclusion of any part of the disc is done, $b = 0$. This bold curve should be seen as the reference.

To better understand what happens in the Hill sphere, Fig. 4 displays the mass distribution in the Hill sphere of the planet, at the moment where the planet is released, computed using the following expression:

$$M_{\rm H}(b) = \int_{s=0}^{+\infty}\int_{\theta=0}^{2\pi} \Sigma\ (1 - f_b(s))\ s{\rm d}\theta\,{\rm d}s\ . \qquad (7)$$

If, instead of the smooth f_b function, a Heaviside function was used, $M_{\rm H}(b)$ would have the more intuitive following expression:

$$M_{\rm H}(b) \approx \int_{s=0}^{br_H}\int_{\theta=0}^{2\pi} \Sigma\ s{\rm d}\theta\,{\rm d}s\ .$$

If Σ was constant, $M_{\rm H}(b)$ should increase as b^2. This is approximately the case only for $b \leqslant 0.15$, which shows that the density decreases strongly with s for $s > 0.15r_H$. In fact, 90% of the mass is inside $0.55r_H$, which favours the idea that the CPD should be considered as only the inner half of the Hill sphere.

The total mass in the Hill sphere is 0.61% of the planet mass, so that the inertial effect should be very small. In addition, the variation of $M_{\rm H}(b)$ for $b > 0.5$ is only a few percent, so the 20% difference in the migration rates between the cases $b = 0.5$, 0.6, 0.8, and 1.0 cannot be explained by a variation in the mass of the excluded region.

4.1.2. High resolution

In a second experiment, the planet is not released at $t = 300$, but kept on a fixed circular orbit until 375 orbits, the resolution being doubled at time 325 (see Table 1). The planet is then released at 375 orbits, with a resolution of 0.002 (35 cells in a Hill radius, 1000 cells in the surface of a circle of radius $0.51r_H$). The results are displayed in Fig. 5. The curves with symbols were performed using f_b as filter, for various values of b.

The average migration rate is a bit slower than in the previous case. The green dashed curves with × symbols (case $b = 1$) in Figs. 3 and 5 are rather linear, providing a constant migration rate, only given by the torque from the PPD outside of the Hill sphere. This torque should be converged for resolutions of the order of $r_H/10$ (here: 0.0046), as widely assumed in the literature (e.g. D'Angelo et al. 2005). However, the gap profile is slowly evolving with time, so that the torque exerted on the planet at $t = 300$ or 375 orbits differs, independently on the resolution. This time delay is the reason why the green dashed curves with × symbols slightly differ in Figs. 3 and 5.

For the other curves, with narrower filters f_b or full gas selfgravity, their various evolutions between the medium-resolution and high-resolution cases suggest that convergence in the Hill sphere had not been reached at medium resolution. In particular, the different variations of the cases $b = 0.4$ and $b = 0.6$ between Figs. 3 and 5 can hardly be explained by a simple smooth time variation of the disc structure. However, we recall that a convergence study of the CPD structure is certainly interesting but is not within the scope of this paper, focused as it is on the role of the CPD in migration in standard numerical simulations.

With $\delta r/r = 0.002$, all the curves are almost linear, denoting that the CPD structure is better resolved. Then, the role of the filter function can be analysed better. Here, the trend is clear. The larger b, the lower the inertial mass of the planet, and the faster the migration, as expected if excluding a part of the Hill sphere only had an effect on the inertial mass of the planet.

In addition, other shapes of filter are tested. The black dots correspond to a case where $f_b(s)$ has been replaced in Eq. (2) by a Gaussian filter:

$$g(s) = 1 - \exp(-(s/r_H)^2)\ . \qquad (8)$$

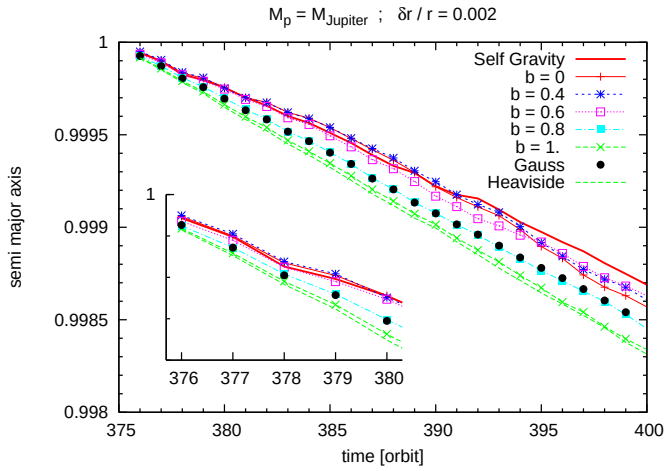

Fig. 5. Migration path of the Jupiter-mass planet after its release at $t = 375$ orbits, with $\delta r/r = \delta\theta = 0.002$. Same colour code as Fig. 3. The five first orbits are enhanced in the inset at the bottom left.

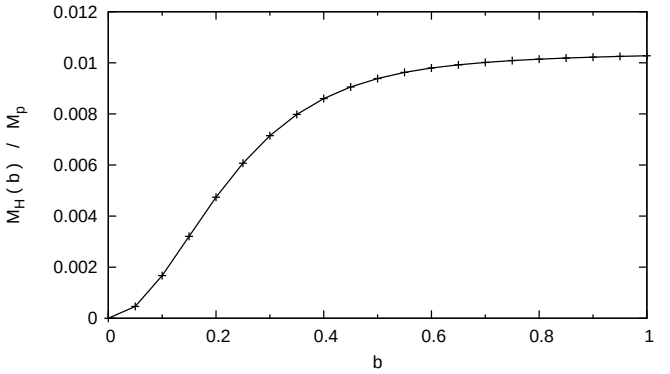

Fig. 6. Mass distribution inside the Hill sphere of the Jupiter mass planet given by Eq. (7), after 375 orbits, with a resolution of $\delta r/r = 0.002$.

It gives almost the same result than $f_{0.8}$ (light blue dot-dashed curve with full squares). The green dashed line without × symbols corresponds to a Heaviside filter $h(s) = 0$ if $s < r_H$, $h(s) = 1$ if $s > r_H$. It gives almost the same result as f_1 (green dashed line with × symbols).

For small b, the difference between $b = 0.6$, $b = 0.4$, $b = 0$, and the full selfgravity case is rather small, although no match is observed. The effect of gas selfgravity on type II migration is little and has nothing to do with its effect on type I migration, which could be expected as the torque felt by the planet in this case is equal to the viscous torque from the disc and not the differential Lindblad torque (which is affected by the gas full selfgravity). Higher values of b, or the use of $g(s)$ or $h(s)$ show a significant acceleration of the migration with respect to the full selfgravity case.

Figure 6 shows the mass distribution inside the Hill sphere of the planet at the moment it is released, after 375 orbits. The distribution is a bit more compact than in previous case: 90% of the mass is now included in $0.48r_H$. The total mass is higher ($0.01\,M_p$). This is due to the doubling of the resolution.

The value of $M_{\rm H}(b)$ does not vary significantly for $b > 0.5$. Consequently, the inertial mass of the planet should not change much whether one half of the Hill sphere is excluded or the full Hill sphere. The acceleration of the migration for $b > 0.6$ is probably not due to the decrease in the inertial mass of the planet. As in the middle resolution case, we find that by excluding all the Hill sphere, one misses a part of the torque that this is not an artifact from the absence of selfgravity.

4.2. Perturbing and gravitational mass problem

The addition of the CPD mass to the perturbing mass of the planet can be easily implemented in the code. One should simply add the mass of the CPD to the planet perturbing mass in computating the gravity potential of the planet through Eq. (1). However, it is not easy to measure the mass of the CPD $M_{\rm CPD}$, because this requires analysing the disc structure. We assume that the CPD is a disc centred on the planet of radius $r \approx 0.6r_H$. Therefore, we take $M_{\rm CPD} = M_{\rm H}(b = 0.6)$. Figures 4 and 6 have shown that the obtained value of $M_{\rm CPD}$ does not vary by more than 10% for $0.5 < b < 1$. The CPD itself should not feel its own mass as added to the planet. This would be inconsistent. Therefore, the expression of the gravitational potential field of the planet is now given by Eq. (1), with

$$M_p^* = M_p + M_{\rm CPD} \times f_b(s)\,, \qquad (9)$$

so that inside br_H, the potential is basically unchanged. Outside, the effective perturbing mass of the planet is $M_p + M_{\rm CPD}$.

Ideally, for $s < br_H$, one should use $M_{\rm H}(s/r_H)$ as defined by Eq. (7) instead of $M_{\rm CPD}\,f_b(s)$. But this is computationally more expensive as it requires calculating $M_{\rm H}(s/r_H)$ for every cell of the grid within a distance br_H to the planet. Alternatively, one could also use a function other than f_b, which would fit the curves displayed in Figs. 4 and 6 better. For consistency, we have kept f_b. This should have only a minor influence on the CPD, and even less on the global simulation. However, it is important that a smooth enough function is used: with a Heaviside-like function, $\Phi_p(s)$ could not be monotonic. In the present case, $f'_{0.6}(s) < 4.2$, while $M_{\rm CPD}/M_p \approx 0.01$, so that the change in $\Phi'_p(s)$ at $s = 0.6r_H$ does not exceed 4%.

With this prescription, we restarted our simulation from $t = 350$ orbits, with the planet on a fixed circular orbit, and a high resolution of $\delta r/r = \delta\theta = 2 \times 10^{-3}$. The mass of the CPD is added smoothly over 3 orbits to the planet mass to avoid a discontinuity: in Eq. (9), $M_{\rm CPD}$ is replaced by $M_{\rm CPD} * g(t)$ with $g(t) = \sin^2((t - 350)\pi/6)$ for $t < 353$ and $g = 1$ for $t \geq 353$.

At 375 orbits, the planet is released and free to migrate, like in Sect. 4.1.2. At this time, the CPD mass is $1.02 \times 10^{-5} M_* = 1\% M_p$, like in Sect. 4.1.2. The result in terms of migration is displayed in Fig. 7 as the curve labelled "large M_p^* ; b=0". The thin red solid curve labelled "$M_p^* = M_p$; $b = 0$" is the most standard simulation, where nothing is done (no full selfgravity, no exclusion, no modification of the masses), also present in Fig. 5. Surprisingly, the migration is slowed down in the first three orbits when the perturbing mass of the planet is increased. The green curve with × symbols corresponds to a case where M_p^* is given by Eq. (9), and in addition $b = 0.6$ in Eq. (2). The black curve with big dots corresponds to a simulation where the perturbing mass is given by Eq. (9) and the gravitational mass of the planet is $M_p + M_{\rm CPD}$. In the first five orbits, adding $M_{\rm CPD}$ to the gravitational mass of the planet or excluding 60% of the Hill sphere both lead to a similar acceleration of the migration: the green and black curves overlap at $t = 380$, below the blue curve. However, in the longer term (20 orbits), these two recipes lead to different migration paths.

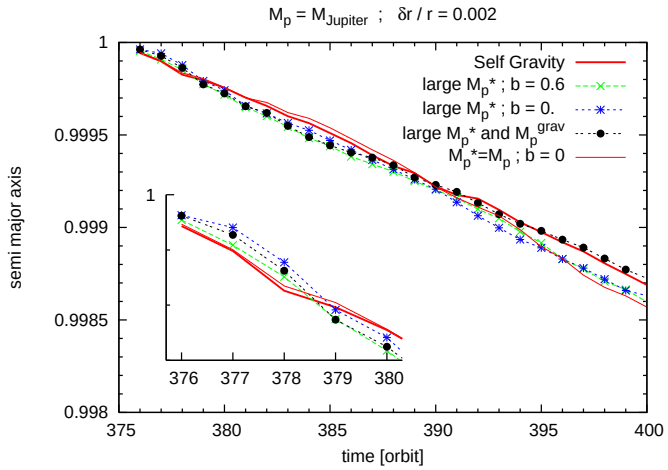

Fig. 7. Migration path of the Jupiter mass planet after its release at $t = 375$ orbits. The label "large M_p^*" denotes simulations for which the planet perturbing mass is given by Eq. (9). The label "large $M_p{}^{\rm grav}$" means that the gravitational mass of the planet is $M_p + M_{\rm CPD}$. The bold curve is the reference case, with full gas selfgravity (and $M_p^* = M_p$).

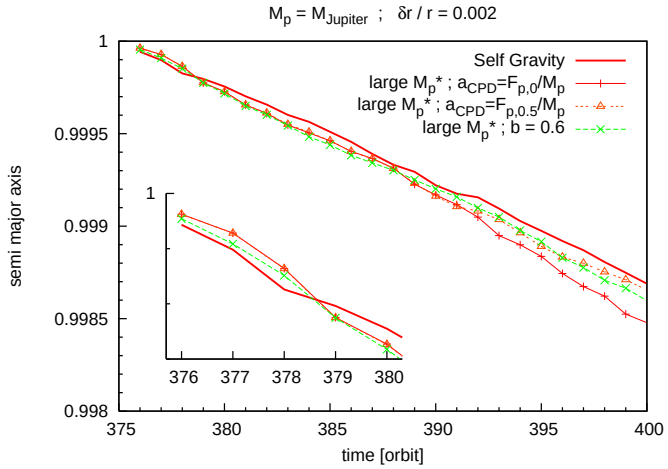

Fig. 8. Migration path of the Jupiter mass planet after its release at $t = 375$ orbits. The perturbing mass of the planet is given by Eq. (9) in every case, except the full selfgravity case (bold solid red line). The acceleration applied to the CPD varies.

4.3. Acceleration of the CPD

Last, we tested the recipe proposed by Pepliński et al. (2008). The perturbing mass of the planet is given by Eq. (9). The force felt by the planet is $\boldsymbol{F}_{\boldsymbol{p},0}$, given by Eq. (2). The acceleration (or the specific force) felt by the planet from the disc is then $\boldsymbol{F}_{\boldsymbol{p},0}/M_p$. This acceleration is then applied to the material inside the Hill sphere, after multiplication by $1 - f_{0.5}(s)$, so the additional acceleration is smoothly vanishing toward zero when $s > 0.5\,r_H$. The material inside $0.5\,r_H$ feels the same acceleration exactly as the planet and should naturally follow the same orbit and the same migration path. This should set the planet free of the "ball and chain" effect of the CPD.

The resulting migration path is shown in Fig. 8 as the red curve with + symbols. The orange curve with open triangles is computed with the same algorithm, except that the acceleration felt by the CPD is the one exerted on the planet by the PPD only, as discussed in Sect. 2.4 : instead of $\boldsymbol{F}_{\boldsymbol{p},0}/M_p$, $\boldsymbol{F}_{\boldsymbol{p},0.5}/M_p$ is applied to the CPD, but the planet still feels $\boldsymbol{F}_{\boldsymbol{p},0}$. During the first 15 orbits, this has only a marginal influence on the migration and the two curves overlap. But after $t = 390$, the paths differ strongly. This proofs that our reasoning in Sect. 2.4 was not vain : it is important to decide whether the acceleration applied to the CPD should include the acceleration of the CPD on the planet or not. The path in the second case is closer to the bold red reference full selfgravity case. We recommend that the acceleration of the CPD on the planet should not be applied to the CPD itself.

The green dashed curve with × symbols is taken from Fig. 7 : M_p^* is given by Eq. (9) in Eq. (1), and $b = 0.6$ in Eq. (2). The green and orange curves are very close but not identical. The acceleration of the CPD or its exclusion of the force exerted by the disc on the planet both give the planet an inertial mass of M_p, but in a different way.

Accelerating the CPD is appealing, because this method gives the planet an inertial mass of M_p, without having to exclude a part of the disc. Moreover, it can be used with the addition of $M_{\rm CPD}$ to the perturbing mass of the planet. However, it does not give the same migration path as the gas full selfgravity either.

4.4. Summary of the type II migration case

We observed the migration rate of a Jupiter mass planet, using various numerical recipe to take the CPD into account. The mass of the CPD is only 1% of the planet mass here, but we find that the way the CPD is considered can change the migration significantly. In particular at lower resolution, excluding a part of the Hill sphere can lead to variations of almost a factor two.

On the other hand, changing the perturbing or gravitational masses of the planet or accelerating the inner half of the Hill sphere leads to a moderate change in the migration speed. The resulting migration path is compatible with the full selfgravity case. Unfortunately, none of the methods leads to the same migration path as when the full selfgravity of the gas is computed.

This suggests that the mass of the CPD was in this case too low to strongly influence the migration, but that the outer layers of the Hill sphere are able to exert a strong torque on the planet. Even if the Hill sphere contains a small amount of gas, it should therefore be considered with care. This is be discussed in more detail in Sect. 6.

5. Type III migration case

The second case that we studied is a Saturn mass planet with $\Sigma_0(r) = 10^{-3} r^{-1/2}\, M_*/{a_p}^2$. This density is one order of magnitude higher than in previous case, so that type III migration is expected for this planet. Indeed, except for what concerns the slope of the density profile, this corresponds to the case studied by Masset & Papaloizou (2003), who found type III migration, and D'Angelo et al. (2005), who claim that type III migration does not happen at high resolution. Another difference with these previous works is that our equation of state is not locally isothermal, which could significantly change the corotation torque (Baruteau & Masset 2008a; Kley & Crida 2008).

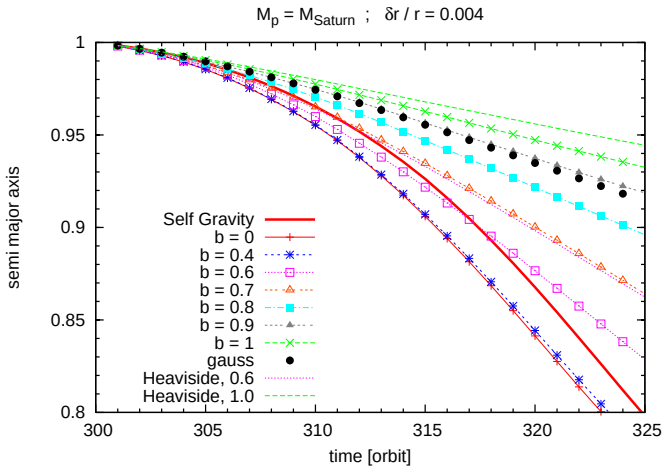

Fig. 9. Migration path of the Saturn mass planet after its release at $t = 300$ orbits. Bold curve : simulation where the gas selfgravity is computed. Curves with symbols : simulations with exclusion of a part of the Hill Sphere, using the filter f_b, for various values of b. Curves without symbols : exclusion of a part of the Hill Sphere with Heaviside filters. Big dots : exclusion of the Hill sphere with a Gaussian filter.

5.1. Inertial mass problem

The same experiment as in the Jupiter mass planet case was performed. The setup was identical, with only the M_p and Σ_0 changed.

5.1.1. Middle resolution

For a restart at 300 orbits and resolution of $4\times10^{-3}a_p = r_H/11.4$, the results are displayed in Fig. 9. The bold, red curve corresponds to the case where the full selfgravity of the gas has been computed. In the other cases, only the axisymmetric component of the selfgravity is computed. The curves with symbols come from simulations with exclusion of a part of the Hill Sphere, using the filter f_b, for various values of b ($b = 0$ means no exclusion). For $b \leqslant 0.3$, the curves overlap and only the case $b = 0$ is drawn. Then, for increasing b, the migration speed decreases.

The black dots correspond to a case where $f_b(s)$ has been replaced in Eq. (2) by the Gaussian filter $g(s)$ given by Eq. (8). It gives almost the same result than $f_{0.9}$ (grey blue short dashed curve with full triangles).

The green dashed line without symbols corresponds to exclusion of the Hill sphere with a Heaviside filter $h(s) = 0$ if $s < r_H$, $h(s) = 1$ if $s > r_H$. It gives the most divergent result with the full selfgravity case. The pink dotted line without symbols corresponds to exclusion of the inner 60% of the Hill sphere with a Heaviside filter $h_{0.6}(s) = 0$ if $s < 0.6\,r_H$, $h_{0.6}(s) = 1$ if $s > 0.6\,r_H$. It gives a result similar to $f_{0.7}$ (orange triple dashed line with open triangles). Not only does the size of the excluded region matters but also the shape of the filter.

First of all, we find that type III runaway migration happens in that case, in agreement with Masset & Papaloizou (2003), even with full selfgravity (bold red line). Admittedly however, we have not reached the resolution of D'Angelo et al. (2005) here (see next section).

Second, when varying b, the migration rate changes dramatically, and for $b \sim 1$, the runaway migration process seems to be broken. This again shows that excluding a part of the Hill sphere or not can have strong consequences on the migration. At $t = 325$ orbits, the semi-major axis of the planet is $a = 0.77$ in the case $b = 0$ and 0.93 in the case $b = 1$. The ratio of the semi major axis variations is 3.33.

Third, the observed behaviour is opposite the expected one if one considers only the inertial mass effect : here the migration speed decreases with b. The total mass of gas included in the Hill Sphere at $t = 300$ orbits is $2 \times 10^{-5}\ M_* = M_p/16$. The impact on the migration speed should thus not be more than 7%. This supports the idea that the observed difference in the migration rate when varying b is not due to a change in the *inertial mass* of the planet, but to the *direct torque* repartition inside the Hill sphere. The mass and torque distribution inside the Hill sphere will be discussed in Sect. 6.

5.1.2. Very high resolution

This simulation is run until $t = 475$ orbits, with the planet on a fixed circular orbit, and increasing resolution following Table 1. The axisymmetric component of the gas gravity is always taken into account. In the end, a resolution of 10^{-3} is reached, so that the length of a Hill radius is covered by 48.2 cells. This is almost exactly the settings of the run 2D5Gb of D'Angelo et al. (2005), for which convergence in resolution was reached. The planet is then released and let free to migrate, excluding a bigger or smaller part of the Hill sphere. The resulting migration paths are displayed in Fig. 10 for various filters.

The migration speed is much slower than at middle resolution (Fig. 9), as already claimed by D'Angelo et al. (2005) (note the different y-axis scale), but the migration rate exponentially increases, in a runaway typical of type III migration. In fact, the difference can arise from two independent effects : (i) as already pointed out for the type II migration case, the disc density profile has evolved with time between $t = 300$ and 475 orbits, independently of the resolution (see Fig. 11). Therefore, the torque felt by the planet at the release date differs. If it is smaller initially (as it appears to be from Fig. 11), the torque remains smaller during the runaway. (ii) The e-folding time of type III migration scales as $CMD/(CMD - M_p)$, where CMD is the coorbital mass deficit, and M_p should be understood as the inertial mass of the planet (see Masset & Papaloizou 2003). Here, the total mass of gas in the coorbital region in the unperturbed disc is about $6\times10^{-4}M_*$, and the value of CMD is of the order of M_p. Therefore, a little increase in the inertial mass of the planet (due to the increase in $M_{\rm CPD}$) results in a significant increase in the e-folding time of the runaway migration. We think that this explains most of the difference between Figs. 9 and 10. The latter effect may also be responsible for the vanishing of type III migration at high resolution in D'Angelo et al. (2005) (Fig. 8) because the mass inside the Hill sphere increases with resolution up to a few M_p, according to their Fig. 9. This shows once again that the Hill sphere should be considered with care. In the type III migration regime, convergence in the Hill sphere structure had better be reached. Here, however, we are not looking for the real migration rate, but for the influence of the gas in the Hill sphere on the migration rate. This experiment is suitable for this purpose.

The major change observed does not stem for a strong modification of the disc structure : the density profile is drawn in Fig. 11 at the two times where the planet is released. The gap width and depth are similar. The CPD is almost twice as massive at very high resolution than at moderate resolution, though, reaching 1% of the planet mass. This promotes the idea that the material in the Hill sphere or the CPD plays a major role in the type III migration rate.

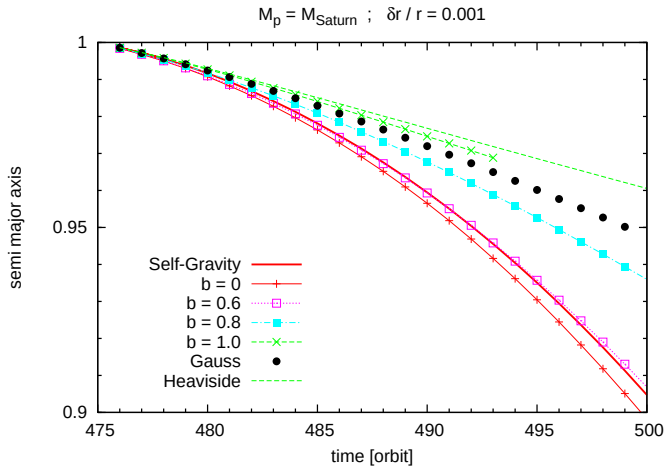

Fig. 10. Migration path of the Saturn-mass planet after its release at $t = 475$ orbits. Bold red curve : the full gas selfgravity is computed. Other curves : only the axisymmetric part of the gas selfgravity is computed. Thin solid red curve with + symbols : the whole disc is taken into account. The other curves come from simulations with exclusion of a part of the Hill sphere, with the filter f_b for various values of b, for the Gaussian filter g, or for the Heaviside filter h.

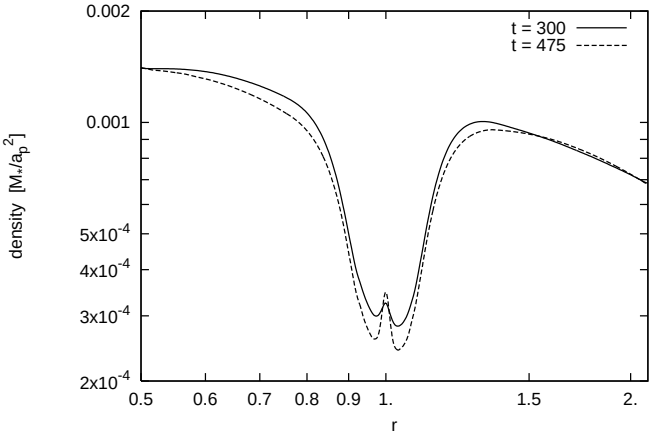

Fig. 11. Density profiles at $t = 300$ orbits ($\delta r/r = \delta\theta = 0.004$) and at $t = 475$ orbits ($\delta r/r = \delta\theta = 0.001$), with a Saturn mass planet on circular orbit at $r = 1$.

In the previous section, the results showed that a large part of the torque responsible for the runaway migration originated in the Hill sphere. Therefore, the lower migration rate observed in a very-high-resolution case leads to the conclusion that the torque exerted on the planet by the material inside the Hill sphere decreases with resolution.

However, for the topic of this paper, we see that even at very high resolution, excluding more than 60% of the Hill sphere has a significant influence on the migration speed. The larger the excluded area, the more the migration diverges with respect to the full selfgravity case. The Heaviside filter to exclude all what is beyond r_H of the planet appears to be the least appropriate.

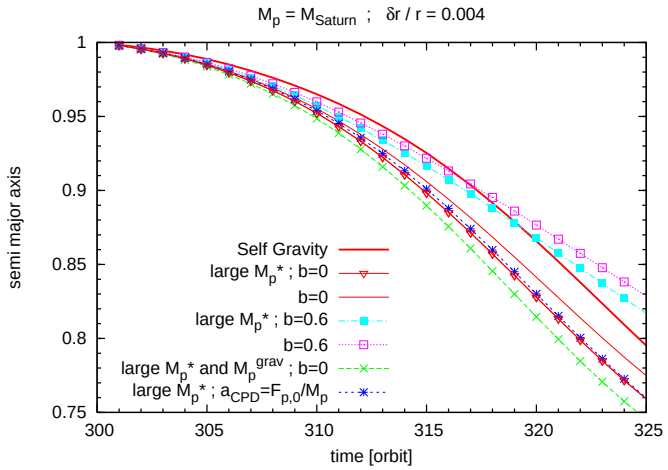

Fig. 12. Migration path of the Saturn mass planet after its release at $t = 300$ orbits, for different perturbing masses. The label "large M_p^*" denotes simulations for which M_p^* is given by Eq. (9) since $t = 290$. The bold curve labelled "Self Gravity" is computed with full gas selfgravity.

5.2. Perturbing and gravitational mass problem, acceleration of the CPD

5.2.1. Middle resolution

With the same prescription as in Sect. 4.2, we restarted our simulation from $t = 250$ orbits, with the planet on a fixed circular orbit and a resolution of 0.004. At this time, $M_{\rm CPD} = M_{\rm H}(0.6)$ has reached $10^{-5}\, M_* = 0.035\, M_p$. It is added smoothly over 40 orbits to M_p^*, to avoid a discontinuity.

Then, we let the planet evolve freely under the influence of the disc at time $t = 300$ orbits. The migration path is shown in Fig. 12 as the red thin solid curve with triangles (labelled "large M_p^* ; b=0"), compared to the migration rate without taking the CPD mass into account (thin red solid curve, labelled "b=0"), and to the selfgravity case (bold solid curve). By excluding in addition the inner 60% of the Hill sphere (*i.e.* taking $b = 0.6$ in Eq. (2)), one gets the light blue, dot-dashed line with full squares (labelled "large M_p^* ; b=0.6"). It can be compared to the similar case, with $M_p^* = M_p$, which is the pink, dotted line with open squares (labelled "b=0.6"). The green dashed curve with × symbols (labelled "large M_p^* and $M_p^{\rm grav}$") corresponds to the last case described in Sect. 2.4 : the perturbing mass is given by Eq. (9), and gravitational mass of the planet is $M_p + M_{\rm CPD}$.

As expected, the migration is accelerated by the augmentation of the perturbing mass of the planet. Adding $M_{\rm CPD}$ to the perturbing mass of the planet leads to a rise in the migration rate of 4% in both cases $b = 0$ and $b = 0.6$. For the 15 first orbits, the curves $a_p(t)$ remarkably overlap if one replaces t by $300 + (t - 300)/1.04$ in the cases with $M_p^* = M_p$. Another 4% increase in the migration speed is observed when $M_{\rm CPD}$ is also added to the gravitational mass of the planet. This is consistent with the mass of the CPD.

The "Self Gravity" simulation was launched at 300 orbits from the same disc as the other simulations here : before $t = 300$ only the axisymmetric component of the selfgravity is computed, and the disc is perturbed by a planetary potential given by Eq. (1) with M_p^* given by Eq. (9). The migration path is almost indistinguishable from the one in the previous section, restarting from the classical potential perturbed disc.

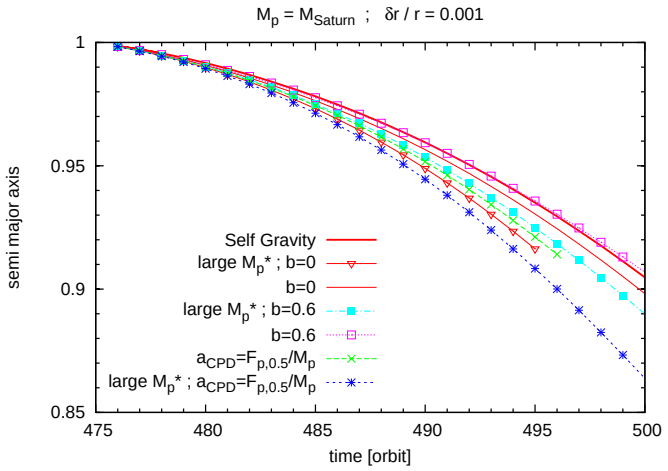

Fig. 13. Migration path of the Saturn mass planet after its release at $t = 300$ orbits. The label "large M_p^*" denotes simulations for which M_p^* is given by Eq. (9) since $t = 290$. The bold curve labelled "Self Gravity" is computed with full gas selfgravity.

Unfortunately, as the full selfgravity case gives a slower migration than the standard simulation, adding the mass of the CPD to the perturbing and gravitational masses of the planet gives an even more divergent result. This means that in this case, the selfgravity plays another role as simply modifying the perturbing, gravitational, and inertial masses of the planet.

As in Sect. 4.3, the algorithm of Pepliński et al. (2008) is also tested and compared to the other ones. The migration obtained with it, with also M_p^* given by Eq. (9), is shown in Fig. 12, as a blue curve with stars, labelled "large M_p^* ; $a_{\rm CPD}$=$F_{p,0}/M_p$". It follows the path of the case with simply M_p^* given by Eq. (9).

5.2.2. Very high resolution

The same experiments are computed at very high resolution from $t = 475$ orbits. At this time, the mass distribution in the Hill sphere of the planet is shown in Fig. 16, and $M_{\rm CPD} = M_H(0.6) = 1.933\times10^{-5}M_* = 0.068M_p$. For the cases with $M_p^* = M_p+M_{\rm CPD}$, the simulation is restarted with this perturbing mass at $t = 450$ orbits, with the planet on a circular orbit until 475 orbits, where the planet is released. As expected, the addition of $M_{\rm CPD}$ to M_p^* accelerates the migration. This can be seen by comparing the thin solid red line to the thin solid red line with open triangles in Fig. 13. These two cases have $b = 0$ but a different perturbing mass. During the 5 first orbits, the migration paths overlap exactly if one replaces t with $475+(t-475)/1.068$ in the $M_p^* = M_p$ case. In the longer term, however, the acceleration of the migration is closer to 10% than 6.8%.

With $b = 0.6$, the influence of the perturbing mass can be seen by comparing in Fig. 13 the pink dotted line with open squares with the light blue dot-dashed line with full squares. The migration rates compare exactly like in the $b = 0$ case : 6.8% difference during the 5 first orbits, 10% in the longer term.

An acceleration of $\boldsymbol{F_p}_{0.5}/M_p$ is then applied to the CPD (green dashed curve with × symbols, labelled "$a_{\rm CPD} = \boldsymbol{F_p}_{0.5}/M_p$"). This leads to an overall acceleration of the migration of about 7% with respect to the standard, $b = 0$ case. This could be expected, but is very different than excluding the CPD from the computation of the force of the disc on the planet (pink dotted curve with open squares). However, both methods aim at delivering the planet from the inertia of the CPD. This shows that they are not equivalent.

If in addition to the CPD acceleration, the perturbing mass is $M_p^* = M_p + M_{\rm CPD}$ (blue dashed curve with stars), the migration is accelerated again. The speed-up is exactly 6.8% with respect to the previous case (acceleration of the CPD with $M_p^* = M_p$) during the first 5 orbits and about 8% in the longer term. Last, in the case where $M_p^* = M_p + M_{\rm CPD}$ and $b = 0$, the acceleration of the CPD leads to a speed-up in the migration of about 5%.

5.3. Summary of the type III migration case

The outer layers of the Hill sphere ($s > 0.6r_H$) play a big role in the type III migration regime. Excluding more than 60% of the Hill sphere leads to a decrease in the migration rate and even to a suppression of the runaway phenomenon. In the full selfgravity simulations, the runaway is present, even at very high resolution, although the migration rate is decreased. Adding $M_{\rm CPD}$ to the perturbing and/or gravitational masses of the planet clearly leads to an acceleration of the migration at the expected rate. Accelerating the CPD appears to have less of an effect at middle resolution, while it plays a significant role at very high resolution.

At middle resolution, no recipe gives a perfect match with the case where the full selfgravity of the gas is computed. We should also conclude that the gas selfgravity plays a more complex role in the type III migration than simply accelerating the CPD or letting the CPD perturb the PPD.

At very high resolution, excluding a part of the Hill sphere also has a strong influence on the migration path. With $b = 0.6$, the agreement with the full selfgravity case is very good. However, this cannot be explained by the analysis of Sect. 2.4, according to which taking $b = 0.6$ should accelerate the migration while it is slowed down here. This agreement is therefore most likely a coincidence. In any case, the type III migration rate is strongly reduced with increased resolution.

6. Direct torque and Hill sphere structure

6.1. Direct torque from the CPD

A short analysis of the direct torque from the CPD, defined as the material bound to the planet, shows that it should be negligible. It has been observed in numerical simulations with grid refinement that two spiral arms form in the CPD, because of tidal effects from the star. Thus, the CPD should not be considered as an axisymmetric structure, but it looks centro-symmetric anyway. At lower resolution, the spiral arms disappear ; however, the axisymmetry of the structure is not perfect. Only the perturbation from the axisymmerty can be responsible from a torque on the planet.

It would be absurd that the CPD alone directly exerts a torque on the planet and makes it migrate on the long term, because the CPD is linked to the planet ; this torque is an internal interaction in the closed {CPD+Planet} system. This system cannot change its orbit by itself. The only possible angular momentum transfer is between the spin angular momentum of the CPD about the planet and the orbital angular momentum of the {CPD+Planet} system about the star, similar to the slow down of the Earth rotation together with increase of the Moon-Earth distance. If one assumes for simplicity that the CPD is a constant density disc of

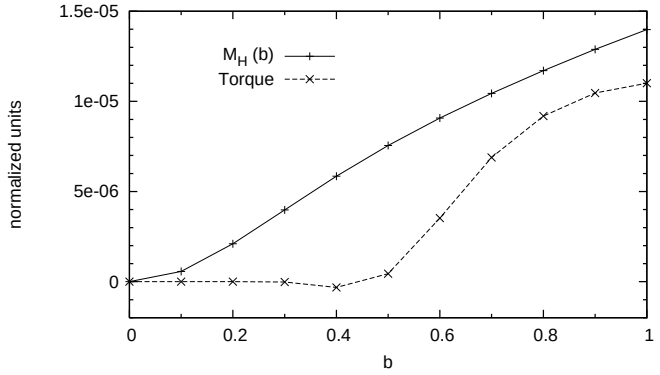

Fig. 14. Mass $M_{\rm H}(b)$ (solid line, Eq. (7)) and Torque (dashed line) distribution in the Hill sphere of the Saturn mass planet at time $t = 300$ orbits.

radius $r_{\rm CPD}$ in Keplerian rotation about the planet, its spin angular momentum is

$$J_{\rm CPD} = \int_0^{r_{\rm CPD}} 2\pi s\Sigma \sqrt{GM_p s}\, {\rm d}s = \frac{4}{5} M_{\rm CPD} \sqrt{GM_p}\sqrt{r_{\rm CPD}}\,. \quad (10)$$

The orbital angular momentum of the planet is $J_p = M_p\sqrt{GM_*}\sqrt{a_p}$. The radius of the CPD is generally of the order of $0.4r_H$. Thus $J_{\rm CPD}/J_p \approx 0.5(M_{\rm CPD}/M_p)q^{2/3}$. Even in the case of a CPD as massive as the planet and of a 3 Jupiter mass planet, the ratio would be inferior to 1%. In the cases studied in Sects. 4 and 5, one finds $J_{\rm CPD}/J_p \approx 5\times10^{-4}$. Thus, the spin angular momentum of the CPD is negligible with respect to the orbital angular momentum of the planet, and consequently the tidal effects of the star (or the PPD) on the latter can only have a negligible effect on the planetary migration.

6.2. Mass and torque distribution inside the Hill sphere

We consider the situation after 300 orbits in the case of a Saturn mass planet in a massive disc for the middle resolution. Figure 14 displays the mass inside the Hill sphere $M_{\rm H}(b)$. It increases significantly with b even for $b > 0.4$, because the gap opened by the planet is not empty (see Fig. 11) ; the background density is responsible for the increase in $M_{\rm H}$ with b. However, the azimuthally averaged profiles shown in Fig. 11 show that a CPD is present.

The torque exerted on the planet by the region within $s < br_H$, is also plotted in Fig. 14 as a function of b. More precisely, it is the torque of the force computed with Eq. (2), with $(1-f_b(s))$ instead of $f_b(s)$; or equivalently the torque of the force : $\boldsymbol{F}_{\boldsymbol{p},0} - \boldsymbol{F}_{\boldsymbol{p},b}$. It appears that for a planet on a fixed circular orbit, the region inside $r_H/2$ exerts a negligible torque, while the region between $r_H/2$ and r_H has a non negligible effect on the planet : the *direct torque* is not small.

Figure 15 shows the torque exerted on the planet by various regions of the disc, as a function of time, during the type III migration between 300 and 325 orbits. The measures are done in the simulation with full gas selfgravity computed. The total torque, exerted by all the disc, is increasingly negative, which is characteristic of runaway inward migration (solid line). The other curves are the torques due to spheres centred on the planet inside the Hill sphere, like in Fig. 14. In the bottom panel, the torques due to fractions of the Hill sphere are plotted in terms of percentage of the total torque. The torque exerted by the material inside the Hill sphere is positive before the planet is released, but

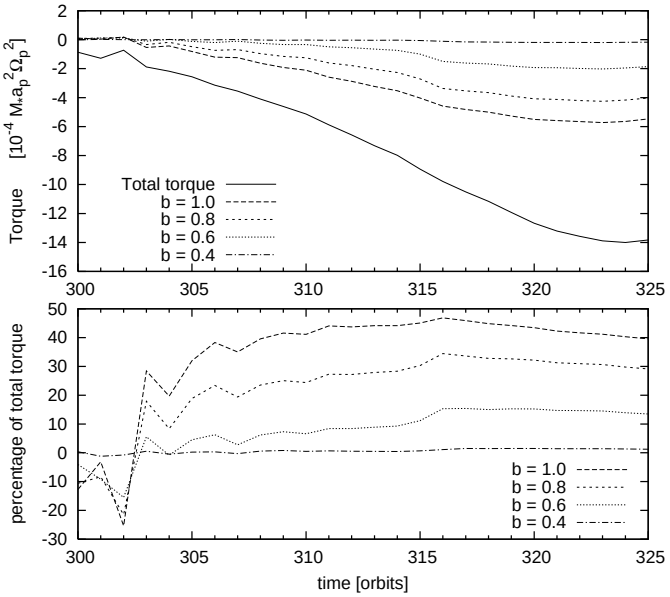

Fig. 15. Torque exerted on the planet as a function of time, during its migration, by all the disc (bottom, solid line), the Hill sphere (dashed line $b = 1.0$), the inner 80% of the Hill sphere ($b = 0.8$), 60% ($b = 0.6$), and 40% ($b = 0.4$). Bottom panel : the same torques as a percentage of the total torque.

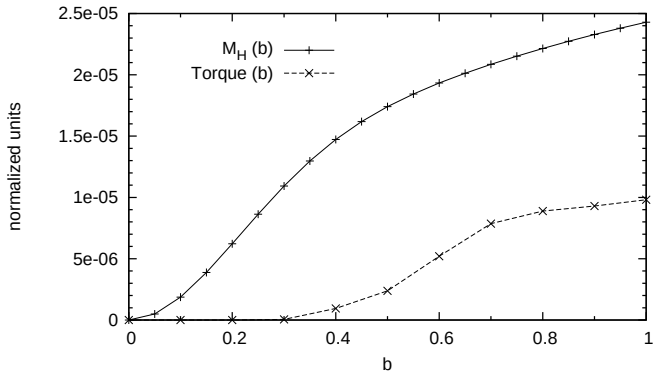

Fig. 16. Mass $M_{\rm H}(b)$ (solid line, Eq. (7)) and torque (dashed line) distribution in the Hill sphere of the Saturn mass planet at time $t = 475$ orbits.

then turns negative. The inner 40% of the Hill sphere plays a negligible role for a migrating planet too. But the entire Hill sphere is responsible for about 40% of the total torque. This confirms that the region between $s = r_H/2$ and $s = r_H$ plays a major role in the process of type III migration, as Fig. 9 suggests.

Figures 16 and 17 are the same as Figs. 14 and 15, but from time 475 orbits on, with the very high resolution. The torques as a function of time in Fig. 17 come from the simulation with only the axisymmetric component of the selfgravity taken into account, and no exclusion of any part of the Hill sphere. The two figures look very similar to the previous ones, in particular the total torque is smaller but is also increasingly negative. The other previous remarks also apply at very high resolution.

6.3. Size of the circum-planetary disc

The calculation results and the analysis of the mass and torque distributions inside the Hill sphere suggest that the region within

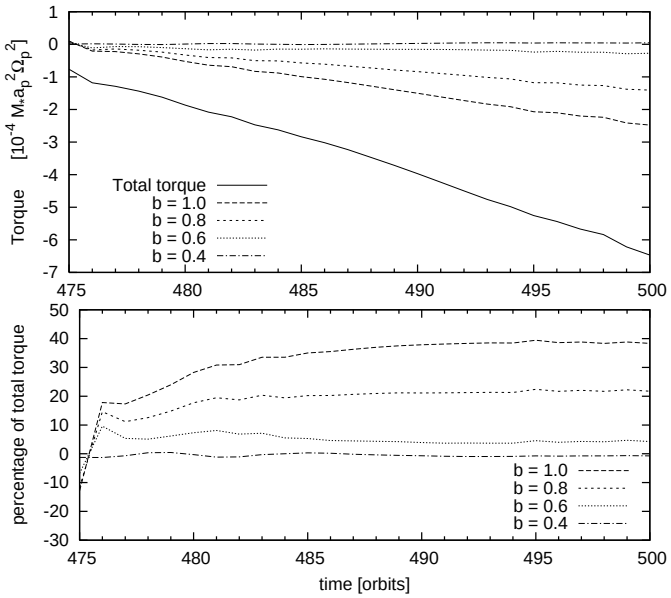

Fig. 17. Torque exerted on the planet as a function of time, during its migration, by all the disc (bottom, solid line), the Hill sphere (dashed line $b = 1.0$), the inner 80% of the Hill sphere ($b = 0.8$), 60% ($b = 0.6$), and 40% ($b = 0.4$). Bottom panel : the same torques as a percentage of the total torque.

$0.5\,r_H$ of the planet contains most of the mass and yet it exerts a negligible torque on the planet, whereas the region between $0.5\,r_H$ and r_H has a negligible mass but it exerts a large torque on the planet. Such a large torque cannot be permanently exerted by material bound to the planet, otherwise this material would not migrate at the same rate as the planet's, and it would ultimately escape from the planet's potential well. This suggests that the CPD is located inside $0.5\,r_H$, which can be checked with a streamline analysis, as shown below. Alternatively, one can determine the shape and the size of the CPD with the following energetic approach. We denote by $E_{\rm tot}$ the total specific energy of the fluid elements perturbed by the planet. It is the sum of the potential, kinetic, and thermal perturbed energies by unit mass of the fluid elements :

$$E_{\rm tot} = -GM_p/s' + |\boldsymbol{v} - \boldsymbol{v_p}|^2/2 + (T - T_0)/(\gamma - 1)\,, \qquad (11)$$

where $\boldsymbol{v} - \boldsymbol{v_p}$ is the velocity with respect to the planet, and $T - T_0$ is the perturbed temperature with respect to the initial state. The minimum energy that the fluid elements must have to leave the planet's potential well with zero velocity with respect to the planet defines the escape energy, denoted by $E_{\rm esc}$. It reads

$$E_{\rm esc} = -GM_p/d'_{\rm stag} + (T - T_0)_{d_{\rm stag}}/(\gamma - 1)\,, \qquad (12)$$

with $d'_{\rm stag} = \sqrt{d^2_{\rm stag} + \epsilon^2}$ the smoothed separation between the planet and one of the two hyperbolic stagnation points (where the velocity of the flow with respect to the planet cancels out). Fluid elements such that $E_{\rm tot} < E_{\rm esc}$ should be bound to the planet, and thus be part of the CPD, whereas those having $E_{\rm tot} \geq E_{\rm esc}$ should orbit the central star. Said differently, the shape and the size of the CPD should correspond to the locations in the disc where $E_{\rm tot} = E_{\rm esc}$.

We first compare both approaches to determine the CPD shape with the middle-resolution run for the Saturn mass planet. In the top panel of Fig. 18, we depict the gas surface density at 300 orbits, just before the planet release. The latter is located

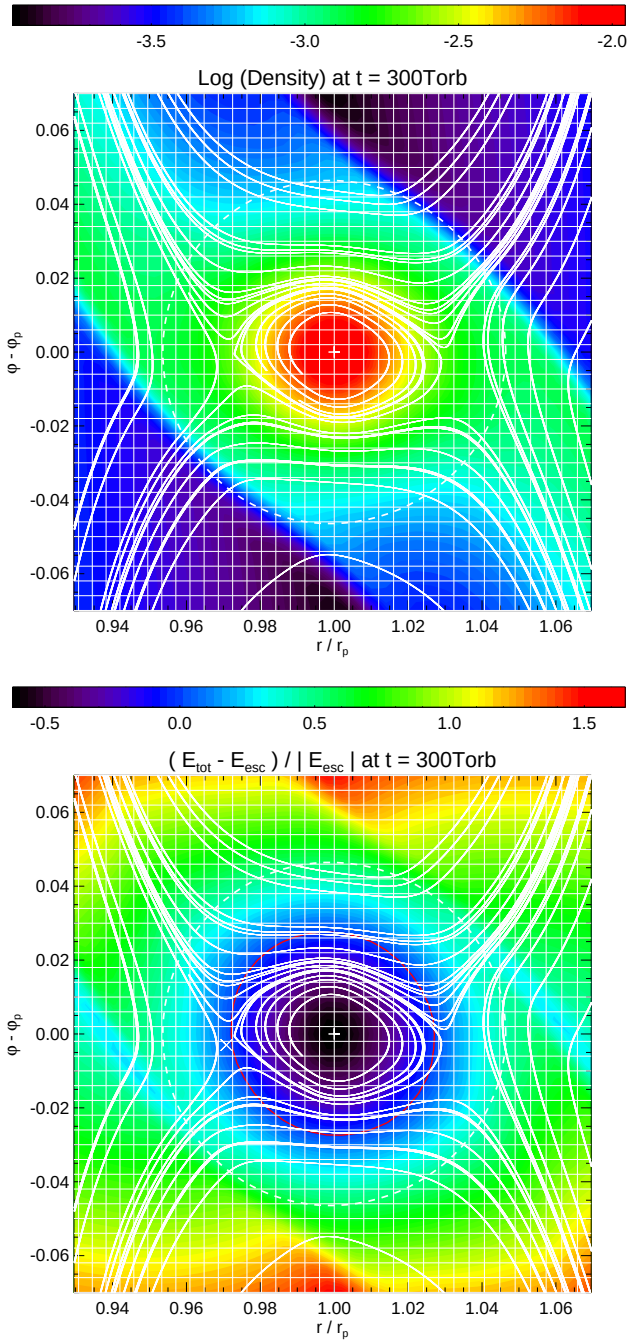

Fig. 18. Top : surface density contour at 300 orbits for the middle-resolution run with the Saturn-mass planet. The planet and its Hill sphere are respectively represented by the + symbol and the dashed circle. The grid mesh is superimposed, as well as streamlines in the planet's frame. Bottom : same as the top panel, except the quantity $(E_{\rm tot} - E_{\rm esc})/|E_{\rm esc}|$ is now displayed. The red solid curve shows the contour $E_{\rm tot} = E_{\rm esc}$, and the $\times$ symbol shows the location of the stagnation point used to evaluate the escape energy $E_{\rm esc}$.

at $r = r_p$ and $\varphi = \varphi_p$, and its position is highlighted with a + symbol. The background vertical and horizontal lines show the grid mesh. The dashed circle represents the planet's Hill sphere. Streamlines (solid curves) are also superimposed to appreciate the shape and the size of the CPD. The streamline analysis confirms that most of the mass inside the planet's Hill sphere is con-

fined to the CPD, and it shows that the latter has an elliptical shape, with a semi-major axis approximately twice as large as the semi-minor axis. The semi-major axis is $\sim 0.6\,r_H$. This justifies that the material inside $\sim 0.5\,r_H$ exerts a small torque on the planet compared to the material located between $0.5\,r_H$ and r_H.

In the bottom panel of Fig. 18, we display the quantity $(E_{\rm tot} - E_{\rm esc})/|E_{\rm esc}|$ at the same time. The same streamlines as in the top panel are depicted. The red solid line shows the contour $E_{\rm tot} = E_{\rm esc}$, the quantity $E_{\rm esc}$ being calculated with Eq. (12). The location of the stagnation point, depicted with a $\times$ symbol in this panel (at $r \approx 0.97 r_p$, $\varphi \approx \varphi_p$), is inferred from the streamline analysis. The contour $E_{\rm tot} = E_{\rm esc}$ can be approximated as a circle of radius $0.6\,r_H$. Its location agrees with that of the CPD determined with the streamline analysis.

Figure 19 is the same as Fig. 18, but for the very high-resolution run just before the release of the Saturn mass planet at 475 orbits. A close comparison between both figures reveals significant differences in the flow topology near the planet. In particular, the CPD is now very close to a circle of radius $0.5\,r_H$, and its shape and its size are in very good agreement with those of the contour $E_{\rm tot} = E_{\rm esc}$. The flow also tends to show more complexity at higher resolution, judging from the presence of a single vortex slightly inside the planet's orbit.

The CPD is slightly larger than in previous locally isothermal studies by D'Angelo et al. (2005). This probably comes from the structure inside the Hill sphere changeing when one changes the equation of state, as the pressure support is modified. With the energy equation, the collapse of the CPD is limited by the heating due to adiabatic compression, which may give a wider but less massive CPD than in the locally isothermal case. Also, the smoothing length ϵ influences the mass and size of the CPD : the smaller ϵ, the deeper the potential well of the planet, and then the larger the CPD. The choice of the equation of state, opacity, and smoothing length certainly influences the size and mass of the CPD. The analysis performed in this section concerns only the specific cases that we studied in this paper, in order to compare the mass and torque repartition in the Hill sphere with the migration rates observed.

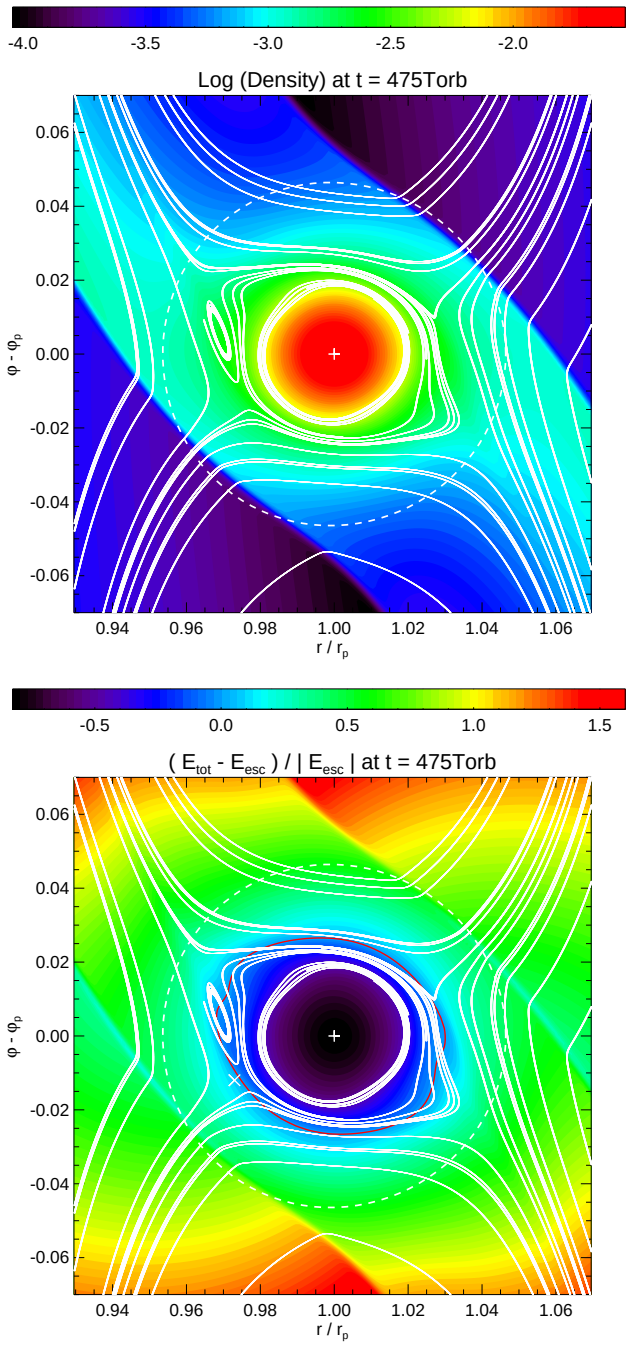

Fig. 19. Same as Fig. 18, but for the very-high-resolution run, just before the release of the planet at 475 orbits. To improve legibility, the grid mesh is not displayed.

7. Conclusion

In this study, we have performed experiments to analyse the role of the circum-planetary disc and the gas in the Hill sphere in the numerical simulations of planetary migration of giant planets. The way the material inside the Hill sphere is taken into account has a strong influence on the outcome of simulations in which the gas selfgravity is not computed. Whether or not a part of the Hill sphere is excluded in the computation of the force felt by the planet, the migration rate can vary by a factor 2 in type II migration, and even 3.33 in case of type III migration. This numerical issue is thus critical. Therefore, we would like to encourage authors to specify how they deal with the Hill sphere of giant planets in their simulations, so that their experiments can be reproducible by others.

In Sect. 2.4, we analysed the problem and proposed several solutions. To deliver the migrating planet from the ball and chain effect of the CPD, it is possible to exclude a part of the Hill sphere from the computation of the force exerted by the disc on the planet. It is also possible to artificially give the CPD the acceleration felt by the planet. Both methods are not equivalent. In order to take the CPD into account in the perturbation of the PPD, the mass of the CPD can be added to the perturbing mass of the planet. In the second case studied here, this leads to an acceleration of the migration proportional to the mass of the CPD. To help the planet to pull the CPD, the gravitational mass of the planet can be increased by $M_{\rm CPD}$, which also accelerates the migration as expected. These four tricks can be combined.

We would like to point out again that the CPD is not the entire Hill sphere. As demonstrated in Sect. 6.3, its size is only about a half of the Hill radius only. As a consequence, excluding all the Hill sphere of the planet is inappropriate ; in fact, our simulations show that this method gives the most divergent results with respect to our reference case (full gas selfgravity computed). Unfortunately, no method matches the full selfgravity case. The role of the selfgravity is more complex than changing the inertial, perturbing, and gravitational masses of the planet.

The present study was conducted for a specific equation of state and for a specific value of the softening length. Under these circumstances, it seems appropriate to remove about half of the Hill sphere in the computation of the force felt by the planet from the disc, but not more than $0.6r_H$. Authors who consider different prescriptions should undertake a prior analysis of the CPD size to infer how they should scale this fraction in their case. Alternatively, accelerating the material within $\sim 0.5\,r_H$ of the planet also provides satisfactory results, but the acceleration imposed on the CPD should be the one provided to the planet by the disc outside $0.5r_H$. The addition of $M_{\rm CPD}$ to the perturbing mass of the planet also seems to be a good idea and leads to an acceleration of the migration. Of course, the most reliable solution is to compute the full gas selfgravity, with the highest resolution possible. In any case, one should be aware of the strong influence of the CPD on planetary migration.

Acknowledgements. A. Crida acknowledges the support through the German Research Foundation (DFG) grant KL 650/7. The high-resolution computations were performed on the `hpc-bw` and `hpc-uni` clusters of the Rechenzentrum of the University of Tübingen.

References

Baruteau, C. & Masset, F. 2008a, ApJ, 672, 1054
Baruteau, C. & Masset, F. 2008b, in AAS/Division of Dynamical Astronomy Meeting, Vol. 39, AAS/Division of Dynamical Astronomy Meeting, #03.03–+
—. 2008c, ApJ, 678, 483
Crida, A. 2006, PhD thesis, Observatoire de la Côte d'Azur, NICE, France
Crida, A. & Morbidelli, A. 2007, MNRAS, 377, 1324
Crida, A., Morbidelli, A., & Masset, F. 2006, Icarus, 181, 587
Crida, A., Sándor, Z., & Kley, W. 2008, A&A, 483, 325
D'Angelo, G., Bate, M. R., & Lubow, S. H. 2005, MNRAS, 358, 316
De Val-Borro, M., Edgar, R. G., Artymowicz, P., et al. 2006, MNRAS, 370, 529
Goldreich, P. & Tremaine, S. 1979, ApJ, 233, 857
Kley, W. & Crida, A. 2008, A&A, 487, L9
Lin, D. N. C. & Papaloizou, J. 1979, MNRAS, 186, 799
—. 1986a, ApJ, 307, 395
—. 1986b, ApJ, 309, 846
Masset, F. 2000a, A&AS, 141, 165
Masset, F. 2000b, in ASP Conf. Ser. 219: Disks, Planetesimals, and Planets, ed. G. Garzón, C. Eiroa, D. de Winter, & T. J. Mahoney, 75–80
Masset, F. 2006, in Tidal interactions in composite systems, ed. M.-J. Goupil & J.-P. Zahn
Masset, F. S. 2001, ApJ, 558, 453
Masset, F. S., D'Angelo, G., & Kley, W. 2006, ApJ, 652, 730
Masset, F. S. & Papaloizou, J. C. B. 2003, ApJ, 588, 494
Meyer-Vernet, N. & Sicardy, B. 1987, Icarus, 69, 157
Nelson, A. F. & Benz, W. 2003, ApJ, 589, 556
Paardekooper, S.-J. & Mellema, G. 2006, A&A, 459, L17
Pepliński, A., Artymowicz, P., & Mellema, G. 2008, MNRAS, 386, 164
Pierens, A. & Huré, J.-M. 2005, A&A, 433, L37
Pierens, A. & Nelson, R. P. 2008, A&A, 482, 333
Ward, W. R. 1986, Icarus, 67, 164
Ward, W. R. 1991, in Lunar and Planetary Institute Conference Abstracts, 1463–1464
—. 1997, Icarus, 126, 261